




## Article

# Preparation and Properties of High Sound-Absorbing Porous Ceramics Reinforced by In Situ Mullite Whisker from Construction Waste

Kaihui Hua <sup>1,2,3</sup> , Xiaobing Chen <sup>1</sup>, Anze Shui <sup>2,\*</sup>, Xiuan Xi <sup>4,\*</sup>, Pinhai Gao <sup>1,3</sup> , Yu Zheng <sup>1,3</sup>  and Chuncan He <sup>1,3</sup>

<sup>1</sup> School of Environment and Civil Engineering, Dongguan University of Technology, Dongguan 523808, China; huakh@dgut.edu.cn (K.H.); chen\_xb4869@163.com (X.C.); gaoph@dgut.edu.cn (P.G.); zhengy@dgut.edu.cn (Y.Z.); hechuncan@dgut.edu.cn (C.H.)

<sup>2</sup> School of Materials Science and Engineering, South China University of Technology, Guangzhou 510641, China

<sup>3</sup> Guangdong Provincial Key Laboratory of Intelligent Disaster Prevention and Emergency Technologies for Urban Lifeline Engineering, Dongguan 523808, China

<sup>4</sup> School of Physical Sciences, Great Bay University, Dongguan 523000, China

\* Correspondence: shuianze@scut.edu.cn (A.S.); xixiuan@163.com (X.X.)

**Abstract:** Porous sound absorption ceramic is one of the most promising materials for effectively eliminating noise pollution. However, its high production cost and low mechanical strength limit its practical applications. In this work, low-cost and in situ mullite whisker-reinforced porous sound-absorbing ceramics were prepared using recyclable construction waste and Al<sub>2</sub>O<sub>3</sub> powder as the main raw materials, and AlF<sub>3</sub> and CeO<sub>2</sub> as the additives, respectively. The effects of CeO<sub>2</sub> content, AlF<sub>3</sub> content, and sintering temperature on the microstructure and properties of the porous ceramics were systematically investigated. The results showed that a small amount of CeO<sub>2</sub> significantly promoted the growth of elongated mullite crystals in the resultant porous ceramics, decreased the growth temperature of the mullite whiskers, and significantly increased the biaxial flexural strength. When 2 wt.% CeO<sub>2</sub> and 12 wt.% AlF<sub>3</sub> were added to the system, mullite whiskers were successfully obtained at a sintering temperature of 1300 °C for 1 h, which exhibited excellent properties, including an open porosity of 56.4 ± 0.6%, an average pore size of 1.32–2.54 μm, a biaxial flexural strength of 23.7 ± 0.9 MPa, and a sound absorption coefficient of >0.8 at 800–4000 Hz.

**Keywords:** construction waste; porous ceramics; whisker skeleton; sound-absorbing; reinforce



**Citation:** Hua, K.; Chen, X.; Shui, A.; Xi, X.; Gao, P.; Zheng, Y.; He, C.

Preparation and Properties of High Sound-Absorbing Porous Ceramics Reinforced by In Situ Mullite Whisker from Construction Waste. *Molecules* **2024**, *29*, 3419. <https://doi.org/10.3390/molecules29143419>

Academic Editor: Steven L. Suib

Received: 13 June 2024

Revised: 17 July 2024

Accepted: 18 July 2024

Published: 21 July 2024



**Copyright:** © 2024 by the authors. Licensee MDPI, Basel, Switzerland. This article is an open access article distributed under the terms and conditions of the Creative Commons Attribution (CC BY) license (<https://creativecommons.org/licenses/by/4.0/>).

## 1. Introduction

Due to rapid industrial development, noise pollution has become a major environmental concern. The use of porous sound absorption materials is considered an effective approach to eliminating noise pollution. Generally, sound-absorbing materials include organic polymer porous materials, metallic porous materials, and inorganic porous materials [1–3]. Organic materials are flammable and prone to aging. Metallic materials are expensive and have poor corrosion resistance. The inorganic porous materials [4,5] have excellent properties, such as fire resistance, corrosion resistance, anti-moth properties, and high-porosity. Porous ceramics have received considerable widespread attention, owing to their unique properties. Among the various porous ceramics, porous anorthite-mullite-corundum ceramics [6] have excellent performance characteristics, such as greater high-temperature creep strength, a higher softening point, and a lower expansion coefficient [7], making them promising sound absorption materials [8]. He et al. [3] prepared high-strength porous ceramics by growing magnesium borate whiskers in situ. They found that as whisker content increased, the absorption curve shifted to the low-frequency direction. The absorption coefficient gradually increased, and the absorption coefficient reached 0.58 in the frequency range of 200–1400 Hz. Chen et al. [9] prepared a ceramic foam using a

pore-forming agent with a porosity of > 80% and a maximum sound absorption coefficient of 0.86 in the sound frequency range of 200–4000 Hz. Du et al. [10] used a mixture of surfactants to prepare high-porosity SiO<sub>2</sub> ceramics through direct foaming. The resulting foam ceramics had porosities ranging from 84.61 to 91.35%, compressive strengths ranging from 5.89 to 0.94 MPa, and a maximum acoustic absorption coefficient of 0.69 at the frequency range of 1000–4000 Hz. Generally, kaolin clay [11], feldspar [12], and quartz have been used as the main raw materials to fabricate porous anorthite-mullite-corundum ceramics. However, they have a limited reserve, and are expensive. As a result, researchers have sought new types of abundant and low-cost minerals to replace the starting materials, such as kaolinite gangue [13], construction waste [6,14], and fly ash [15,16]. Among them, construction waste is mainly generated from inorganic non-metallic materials, such as mud and residue generated in the process of building construction, building demolition, and building decoration. Construction waste is produced in large quantities and has a low utilization rate, resulting in various environmental issues [17]. It is rich in alumina, silicon oxide, and similar minerals. As a result, it can be used as the starting material to fabricate porous anorthite-mullite-corundum ceramics, thereby solving the above environmental problems.

For effective sound absorption, the sound absorption materials should have an appropriate open porosity with numerous fine, uniform, and connected pores. Porous ceramics with whiskers or fibers meet these criteria [18,19]. Specifically, the in situ fabricated whisker-reinforced porous ceramics characterized by high open porosities and abundant whisker skeletons are highly effective in obstructing the soundwave and converting the sound energy to thermal energy. Furthermore, the whisker skeletons also enhance the strength of the porous materials [20]. Whisker catalysts (including H<sub>12</sub>AlF<sub>6</sub>N<sub>3</sub> [13], AlF<sub>3</sub> [6], NH<sub>4</sub>F [21], and other fluoride additives) and mineralizing agents (including V<sub>2</sub>O<sub>5</sub> [22], MoO<sub>3</sub> [23], WO<sub>3</sub> [24], and CeO<sub>2</sub> [25]) are used to fabricate the in situ mullite whiskers. Among them, CeO<sub>2</sub>, a rare earth oxide, is used as a high melting point stable additive, and it consistently enhances the mullitization behavior and morphology during the fabrication of mullite whiskers [26,27].

In recent years, preparing porous mullite ceramics using inexpensive industrial wastes to minimize raw material expenses and overall energy consumption has attracted considerable attention from researchers. Wang et al. [20] prepared low-cost porous acoustic ceramics using steel slag and kaolin as raw materials, and V<sub>2</sub>O<sub>5</sub> and AlF<sub>3</sub> as additives to enhance the secondary mullitization reaction at reduced temperatures. The prepared ceramics exhibited impressive characteristics, including an open porosity of 65% and a compressive strength of 6.8 MPa. Huo et al. [28] prepared high-strength mullite whisker porous ceramics by calcining high-alumina fly ash as raw material at 1300 °C. The samples had a high-porosity of 49% and a compressive strength of 13 MPa. Liu and Xiang [29] prepared porous mullite ceramics using photovoltaic silicon waste as the raw material, and ammonium molybdate tetrahydrate as the additive. These materials reduced the reaction temperature of mullitization to 200 °C, and were sintered at 900 °C. The porous mullite ceramics exhibited pore diameters of 0.23 μm and 0.5 μm. Furthermore, these ceramics exhibited a flexural strength of 52.8 MPa, and a porosity of 41.8%.

In this work, CeO<sub>2</sub> was proposed and used as the nucleation agent. Mullite whisker-reinforced porous sound-absorbing ceramics were produced using construction waste and Al<sub>2</sub>O<sub>3</sub> powder as the main raw materials, and AlF<sub>3</sub> as the crystallization catalyst. The effects of CeO<sub>2</sub>, AlF<sub>3</sub>, and sintering temperature on the microstructure and properties of the porous ceramics were systematically investigated. The formation and growth mechanism of the mullite whiskers is also discussed in detail.

## 2. Results and Discussions

Figure 1 illustrates the influence of CeO<sub>2</sub> concentration on the open porosity and biaxial flexural strength of the samples containing 12 wt.% AlF<sub>3</sub>. As illustrated in Figure 1, as the concentration of CeO<sub>2</sub> increased, the open porosity of the samples decreased, whereas the biaxial flexural strength was enhanced. Meanwhile, a small amount of CeO<sub>2</sub> (0–2 wt.%)

significantly enhanced the biaxial flexural strength and slightly reduced the open porosity. As the CeO<sub>2</sub> content increased from 0 to 2 wt.%, the biaxial flexural strength improved by 13.3 MPa, increasing from 29.4 ± 0.8 to 42.7 ± 0.8 MPa, while the open porosity decreased from 55.7 ± 0.6% to 53.2 ± 0.5%, decreasing by 2.5 ± 0.6%. When the content of CeO<sub>2</sub> was further increased, sharp decreases and increases were observed in both the biaxial flexural strength and the open porosity, respectively.

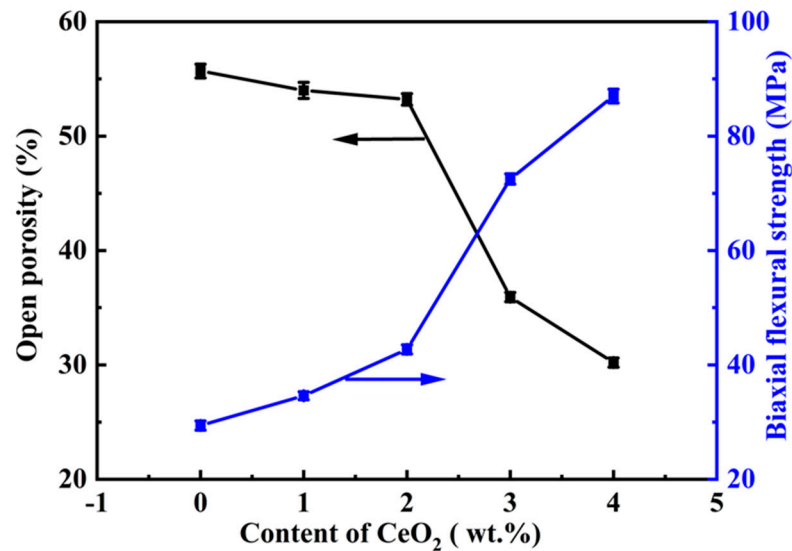


**Figure 1.** Effect of CeO<sub>2</sub> concentrations on the open porosity and biaxial flexural strength of the specimens.

Figure 2 illustrates the bulk density and linear shrinkage rate of specimens containing 12 wt.% AlF<sub>3</sub> and different quantities of CeO<sub>2</sub> (0–4 wt.%). As the CeO<sub>2</sub> content increased, the bulk density and linear shrinkage of the samples slightly decreased in a certain range (0–2 wt.%), and then increased (2–4 wt.%). This phenomenon occurred because a small amount of CeO<sub>2</sub> promoted the mullitization reaction of Al<sub>2</sub>O<sub>3</sub> and SiO<sub>2</sub>, resulting in the production of more mullite whiskers. Compared to spherical or massive particles, the voids between the whiskers were larger, making the filling effect less uniform, and reducing overall bulk density. The uniform distribution of mullite whiskers prevented uneven local shrinkage and stress concentration in porous ceramics, thereby reducing the fluctuation of linear shrinkage. The specimen with 2 wt.% CeO<sub>2</sub> exhibited the lowest bulk density (1.47 g·cm<sup>-3</sup>) and lower linear shrinkage (5.33%). Excess CeO<sub>2</sub> contributed to the formation of a glassy phase in the ceramic materials. The glassy phase had high mobility and could fill the voids and micropores in the ceramic materials during sintering, increasing the bulk density of the ceramics. The glass phase exhibited certain deformation and plasticity, allowing it to flow and deform at high temperatures to fill the microscopic pores during the sintering process of the ceramic material. These deformation and plasticity properties increased the overall linear shrinkage of the ceramic material.

Figure 3 illustrates the X-ray diffraction (XRD) patterns of the samples containing 12 wt.% AlF<sub>3</sub> and varying CeO<sub>2</sub> concentrations (0–4 wt.%). As shown in Figure 3, a large quantity of corundum (Al<sub>2</sub>O<sub>3</sub>, PDF#46-1212) and small amounts of anorthite (CaAl<sub>2</sub>Si<sub>2</sub>O<sub>8</sub>, PDF#41-1486) were detected in the specimens without CeO<sub>2</sub>. As the CeO<sub>2</sub> content increased from 0 to 2 wt.%, the corundum peak intensities weakened, and the mullite and anorthite peak intensities strengthened. Among them, changes in the mullite phase peak intensities were the most prominent. When CeO<sub>2</sub> content increased from 2 to 4 wt.%, all the intensities of the mullite, anorthite, and corundum peaks weakened. According to the literature, the Gibbs free energy of (CaO·Al<sub>2</sub>O<sub>3</sub>·2SiO<sub>2</sub> → 3Al<sub>2</sub>O<sub>3</sub>·2SiO<sub>2</sub>) at elevated temperatures is negative, indicating that calcium feldspar generation of mullite is possible [30]. Therefore, we hypothesize that the presence of CeO<sub>2</sub> facilitates the conversion of calcium feldspar to mullite. Thus, the peak of the calcium feldspar phase weakens with increasing CeO<sub>2</sub>

content. The addition of excess  $\text{CeO}_2$  led to the formation numerous liquid phases, which existed as glassy phases after cooling. The glassy phases covered the surface of the mullite whiskers, thus weakening the mullite and corundum phase peaks [31].

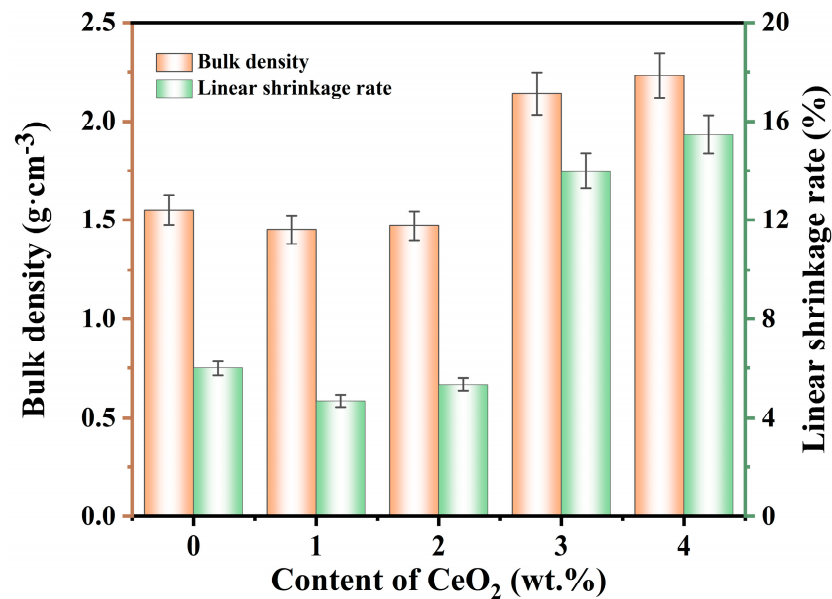


Figure 2. Effect of  $\text{CeO}_2$  concentrations on the bulk density and linear shrinkage rate of the specimens.

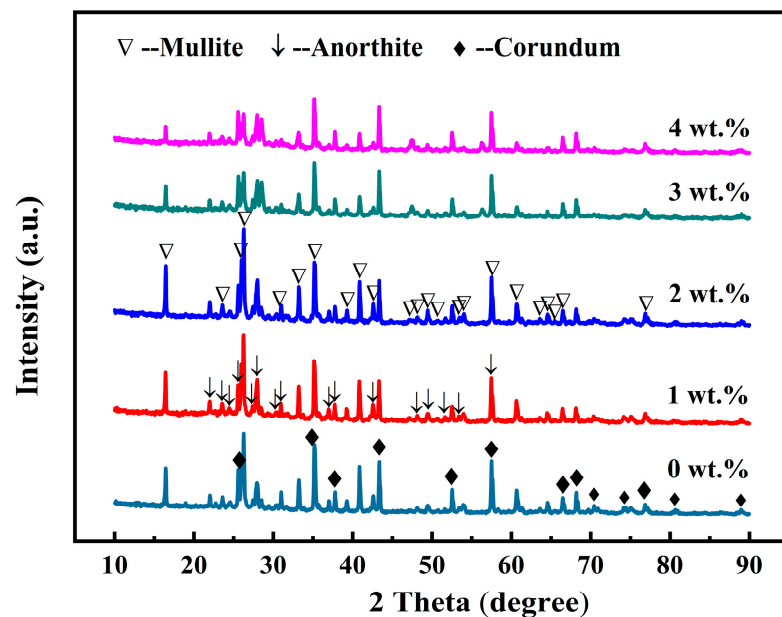
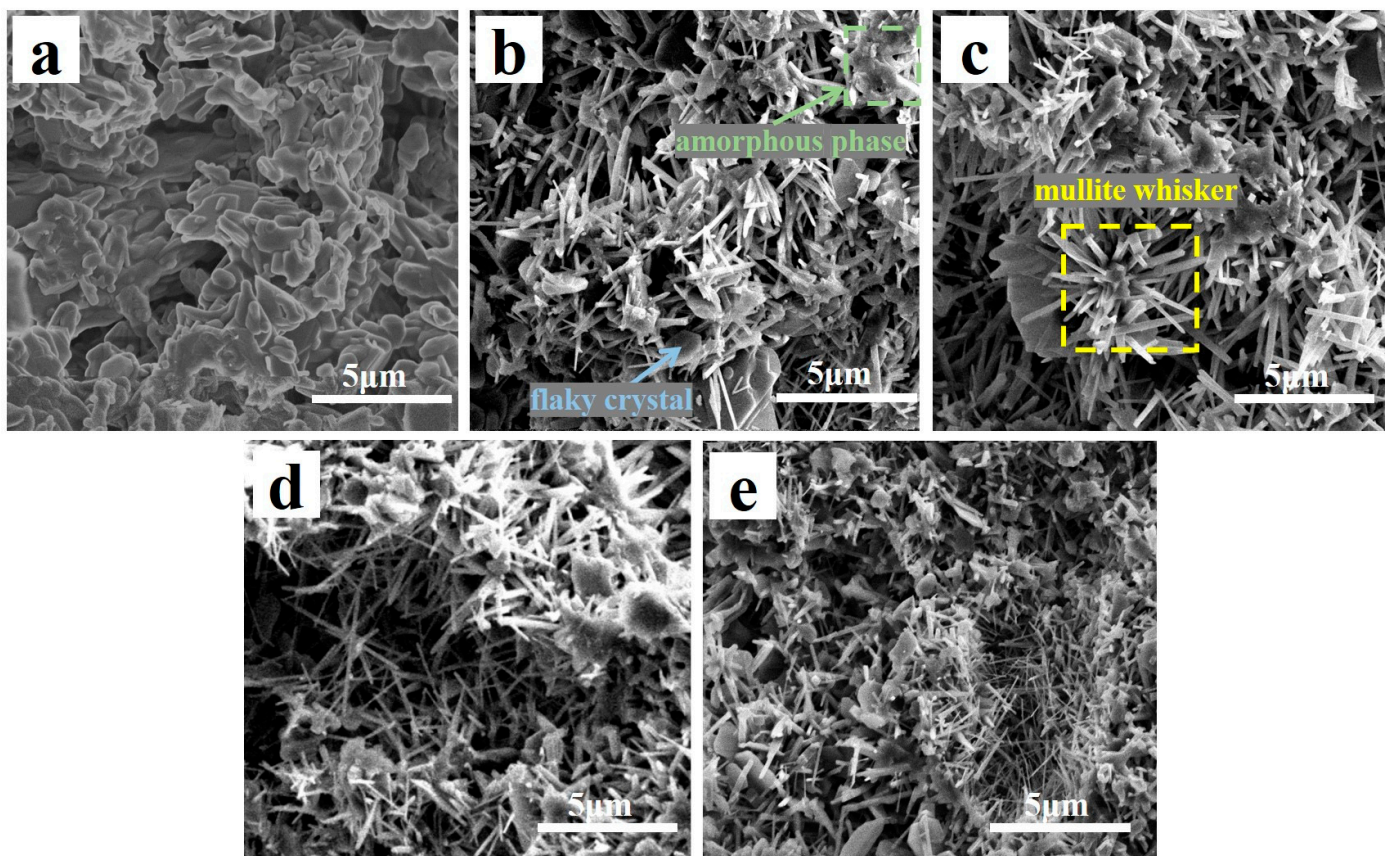


Figure 3. X-ray diffraction patterns of the porous ceramics with different content of  $\text{CeO}_2$ .

Figure 4 shows the SEM images with different  $\text{CeO}_2$  contents (0–4 wt.%) of the samples. Almost no whiskers were detected in the specimens without  $\text{CeO}_2$ , as illustrated in Figure 4a. The samples with 1 wt.%  $\text{CeO}_2$  exhibited a combination of irregularly shaped crystals, small needle-like structures, and some flaky crystals [32] (Figure 4b). When  $\text{CeO}_2$  content was increased to 2 wt.%, the porous structure for the specimens was almost supported by arranging in or forming fascicular whisker columns, while the flake-like crystals vanished, and a small amount of amorphous material was attached to the surface of the fascicular whisker columns (Figure 4c) [33,34]. When  $\text{CeO}_2$  content was increased to 3 wt.%, the whiskers decreased in size, while the amorphous phase increased (Figure 4d). The

quantity and size of whiskers of specimens containing 4 wt.% CeO<sub>2</sub> decreased, while flaky crystals resurfaced (Figure 4e).



**Figure 4.** Fracture surface scanning electron microscopy images of porous ceramics with different concentrations of CeO<sub>2</sub>: (a) 0 wt.%, (b) 1 wt.%, (c) 2 wt.%, (d) 3 wt.%, and (e) 4 wt.%.

Studies have shown that the flake-like crystals comprise  $\alpha$ -Al<sub>2</sub>O<sub>3</sub> [4], and the whiskers are composed of mullite. Analysis of the SEM images presented in Figure 4 reveals that the introduction of appropriate content of CeO<sub>2</sub> to the base materials can accelerate the mullitization process. However, an excessive amount of CeO<sub>2</sub> hindered mullitization, resulting in the formation of a greater proportion of amorphous material. These results are consistent with the XRD results in Figure 3, where the corundum peak intensities decrease, and that of the mullite phases increase with increasing CeO<sub>2</sub> content within a certain range (0–2 wt.%). When CeO<sub>2</sub> content increased from 2 to 4 wt.%, the intensities of mullite, anorthite, and corundum peaks were all weakened. The introduction of CeO<sub>2</sub> into the starting materials promoted the crystallization of mullite grains, which could be attributed to its strongly accelerated reaction bonding process mechanism, and the dissolution–precipitation mechanism [35]. The former mechanism could be detailed as follows: the low Gibbs (0.26 kJ) of the reaction of Al<sub>2</sub>O<sub>3</sub> [15] makes it challenging to naturally form mullite when combining Al<sub>2</sub>O<sub>3</sub> and SiO<sub>2</sub> without activation. The 4f15d16s2 particular atomic structure of Ce made the atom easily lose electrons, and CeO<sub>2</sub> easily released oxygen. Studies have shown that incorporating CeO<sub>2</sub> into the starting material can convert lattice defects of oxygen atoms into activated centers, significantly improving the reaction bonding of mullite from Si and Al<sub>2</sub>O<sub>3</sub> [36]. This change indicates the generation of a low-viscosity Ce–Al–Si–O liquid phase, facilitating species diffusion, accelerating the oxidation of Si metal, and expediting mullite formation. Furthermore, the addition of CeO<sub>2</sub> reduces the nucleation energy necessary for mullite whisker growth, leading to a rapid decrease in activation energy [8]. Once the mullite nuclei reach a critical size, there is a sharp decline in activation energy, leading to the rapid growth of mullite whiskers [37].

The process involving the dissolution–precipitation mechanism is influenced by the size difference between  $\text{Ce}^{4+}$  and  $\text{Al}^{3+}$  ions. Integrating  $\text{Ce}^{4+}$  into the gaps of the  $\text{Al}_2\text{O}_3$  lattice to create a solid solution is challenging due to its larger radius. Consequently,  $\text{Ce}^{4+}$  ions accumulated at the boundaries of mullite grains, impeding grain growth and preventing the formation of secondary phases. This accumulation explains why incorporating an appropriate amount of  $\text{CeO}_2$  into the initial materials increases the production of whiskers and accelerates mullite formation. Conversely, an excess of  $\text{CeO}_2$  hinders crystal growth in one direction, thus decreasing the crystal draw ratio and coarsening of mullite whiskers [26]. Thus, effectively regulating the  $\text{CeO}_2$  content is crucial for the successful fabrication of mullite whiskers.

Figure 5 shows the effect of the sintering temperatures (1150–1400 °C) on the open porosity and biaxial flexural strength of the specimens of A12C2. Increasing the sintering temperature led to a reduction in the open porosity of the specimens, whereas the biaxial flexural strength increased. When the sintering temperature was relatively low (1150–1200 °C), the open porosity and biaxial flexural strength of the specimens slightly changed. Conversely, elevating the sintering temperature from 1300 to 1400 °C resulted in a noticeable change in both the open porosity and biaxial flexural strength of the specimens. When the sintering temperature was increased from 1150 to 1200 °C, the open porosity slightly decreased from  $59.5 \pm 0.6\%$  to  $59.1 \pm 0.5\%$ , while the biaxial flexural strength increased from  $12.1 \pm 0.3$  MPa to  $19.2 \pm 0.8$  MPa. When the sintering temperature was increased from 1300 to 1400 °C, the open porosity decreased from  $56.4 \pm 0.6\%$  to  $14.8 \pm 0.3\%$ , whereas the biaxial flexural strength significantly increased from  $23.7 \pm 0.9$  MPa to  $157.3 \pm 2.3$  MPa.

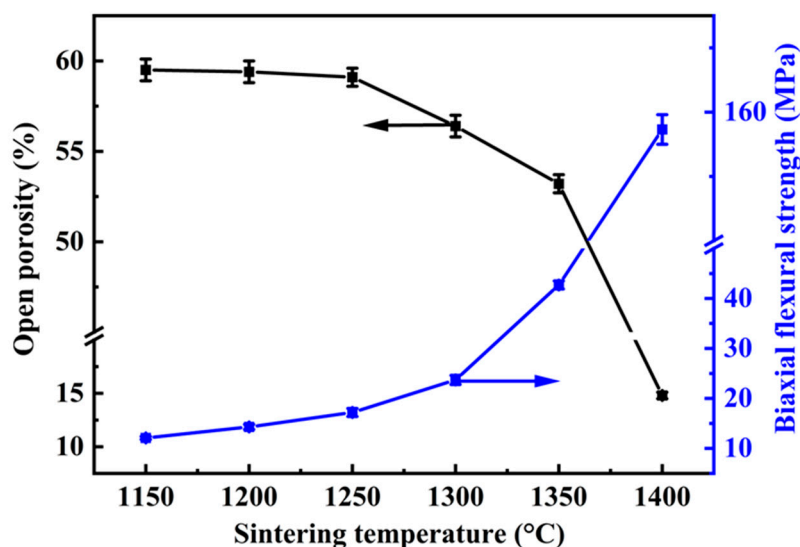


**Figure 5.** Effect of the sintering temperatures on the open porosity and biaxial flexural strength of specimens with 2 wt.%  $\text{CeO}_2$ .

Figure 6 illustrates the trend of linear shrinkage rate and bulk density of the sample A12C2, sintered at different temperatures (1150–1400 °C). The bulk density and linear shrinkage of the specimens exhibited similar trends, corresponding to the sintering temperature. They both maintained a consistent level within the sintering temperature range of 1150–1250 °C. The low-temperature sintering was insufficient to form a good bond between the ceramic particles, leading to the existence of more voids and pores inside the ceramics, which reduced the bulk density and linear shrinkage. When the sintering temperature was increased from 1250 to 1400 °C, the bulk density and linear shrinkage of the specimens gradually increased, and the increase was more significant in the relatively high sintering temperature range (1350–1400 °C). When the sintering temperature was increased from 1150 to 1350 °C, the bulk density of the specimens increased from

1.25 g·cm<sup>-3</sup> to 1.46 g·cm<sup>-3</sup>, and the linear shrinkage increased from 0% to 5.33%. When the temperature was increased to 1400 °C, the bulk density and linear shrinkage increased to 2.53 g·cm<sup>-3</sup> and 23.07%, respectively. High sintering temperatures induced the formation of glassy phases and accelerated inter-particle bonding in porous ceramics, and the pores in the ceramic materials were further filled. As a result, the overall bulk density and linear shrinkage increased.

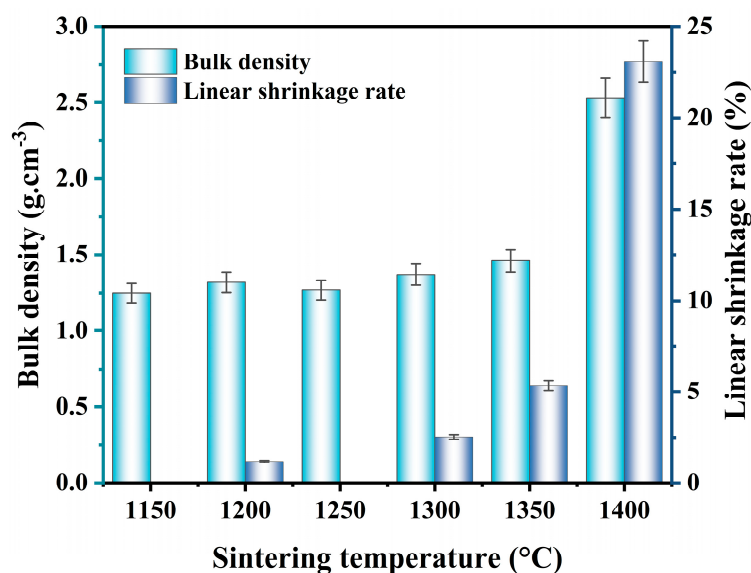


**Figure 6.** Effect of the sintering temperatures on bulk density of the specimens with 12 wt.% AlF<sub>3</sub> and 2 wt.% CeO<sub>2</sub>.

Figure 7 shows the XRD patterns of the specimens of A12C2 sintered at different temperatures (1150–1400 °C). The specimens contained a significant amount of quartz (PDF#46-1045), cerianite (CeO<sub>2</sub>, PDF#43-1002), and a minor amount of albite (NaAlSi<sub>3</sub>O<sub>8</sub>) at 1150 °C. When the sintering temperature was increased to 1200 °C, the quartz peaks diminished, while the albite phase intensities progressively increased, with minimal alterations observed in the cerianite phase peaks. In addition, peaks in the corundum and mullite phases were identified. When the sintering temperature was increased to 1250 °C, anorthite phase peaks appeared, mullite, corundum, and albite peaks became more distinct, and quartz and cerianite peak intensities weakened. At 1300 °C, the mullite and corundum peak intensities significantly increased, and the anorthite peaks slightly changed; however, the albite peaks decreased, and the quartz and cerianite phase peaks disappeared. This phenomenon was attributable to the direct involvement of both the quartz and cerianite phases in the growth of mullite. The albite phase was decomposed to a silicon source or alumina sources, and was indirectly involved in the growth of mullite at a relatively high sintering temperature (1200–1300 °C). When the sintering temperature was increased to 1350 °C, the intensities of the corundum peaks continually increased, while the intensities of all other phase peaks decreased.

Figure 8 shows the SEM images of A12C2 specimens sintered at different temperatures. Randomly shaped blocks were observed in the specimens sintered at 1150 °C (Figure 8a) without patches or whiskers. Some flake-like crystals and whiskers emerged in the specimens sintered at 1200 °C, with irregularly shaped blocks supporting the porous structure (Figure 8b). The XRD patterns of the specimens sintered at 1200 °C (Figure 7) showed peaks of both the mullite and corundum phase, confirming the whiskers' crystals were mullite phase, and most of the flake-like crystals were  $\alpha$ -Al<sub>2</sub>O<sub>3</sub>. When the sintering temperature was increased to 1250 °C, more needle-like whiskers grew, and only a small amount of the patches and glass-like crystals existed (Figure 8c). When the sintering temperature increased to 1300 °C, the flake-like crystals and the glass phases disappeared, and the

porous structure was almost entirely composed of grown needle-like whiskers (Figure 8d). When the sintering temperature increased to 1350 °C, the whiskers coarsened to fascicular whisker columns, and the surface of the fascicular whisker columns was wrapped by the glass phase (Figure 8e). After the sintering temperature was increased to 1400 °C, the whiskers' porous structure hardened to bulk (Figure 8f), which is probably due to the growth the glass phase had surrounding the whiskers, thus filling the porous structure. Thus, the open porosities rapidly decreased, while the biaxial flexural strength rapidly increased (Figure 5).

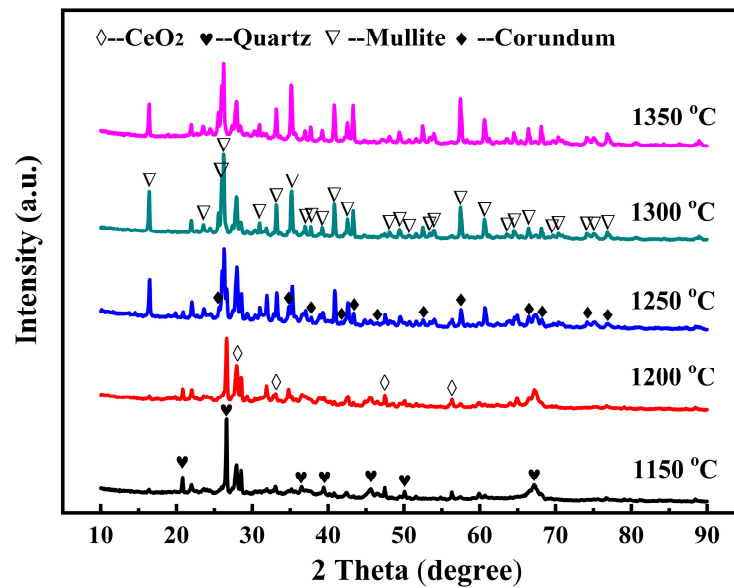


Figure 7. XRD patterns of the specimens of A12C2 sintered at various temperatures for 1 h.

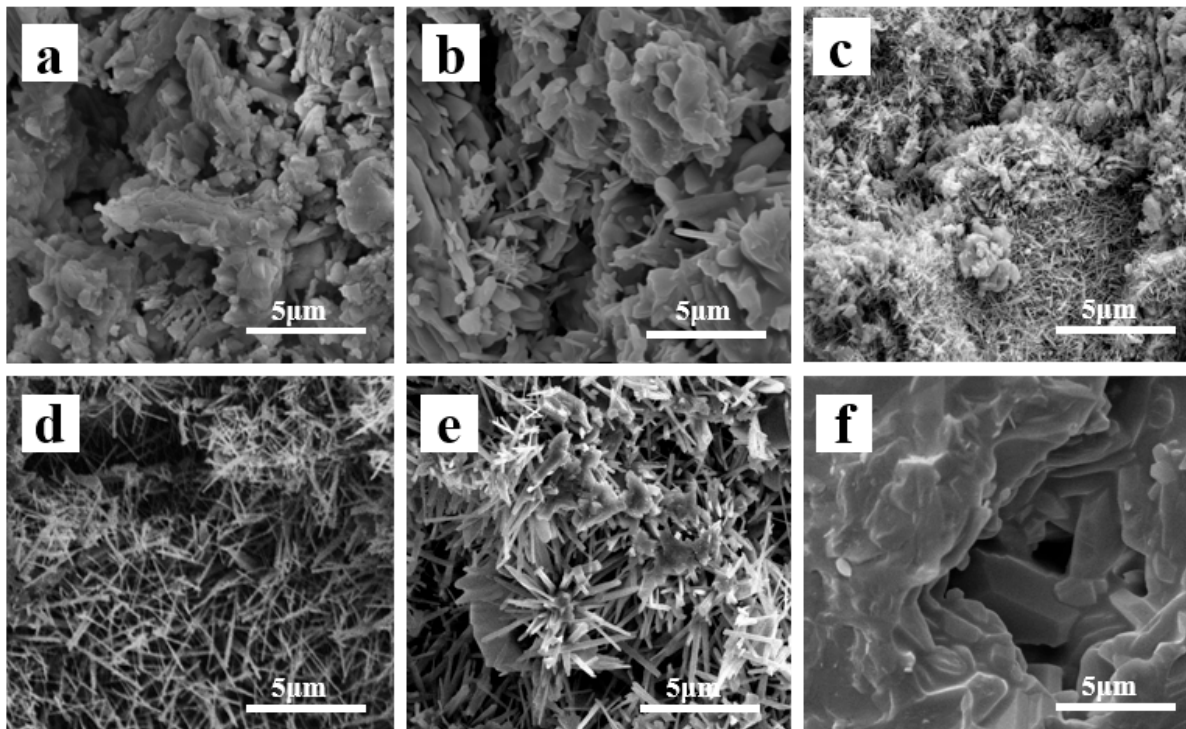
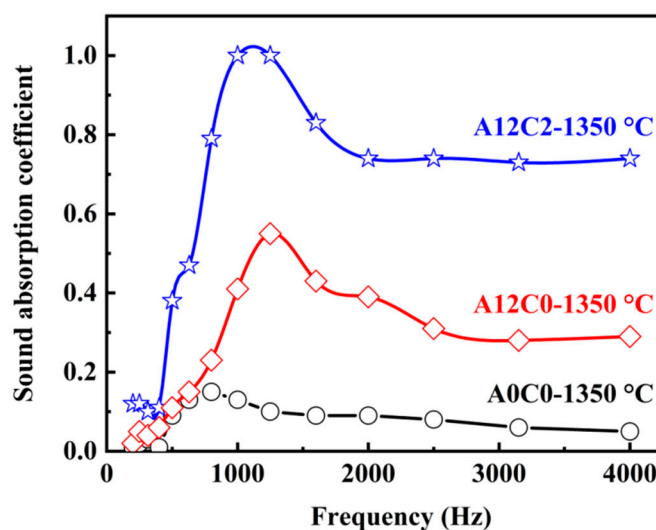


Figure 8. Fracture surface SEM images of the porous ceramics with 12 wt.%  $\text{AlF}_3$  and 2 wt.%  $\text{CeO}_2$  at various temperatures: (a) 1150 °C, (b) 1200 °C, (c) 1250 °C, (d) 1300 °C, (e) 1350 °C, and (f) 1400 °C.



Compared to the additives of  $\text{MoO}_3$  used in the previous work,  $\text{CeO}_2$ , used in this work, is more effective in forming mullite columns, which enhances the bending strength of samples. Meanwhile, the addition of  $\text{CeO}_2$  also effectively decreased the sintering temperature for the samples, and decreased the grown temperature of mullite whiskers. In this work, with 2 wt.%  $\text{CeO}_2$ , the mullite whiskers were detected in the samples sintered at  $1200\text{ }^\circ\text{C}$ , which is  $100\text{ }^\circ\text{C}$  lower than that of the previous work. Moreover, the sintering temperature for the full growth of the mullite whiskers in the porous structure was  $1300\text{ }^\circ\text{C}$ , which is  $50\text{ }^\circ\text{C}$  lower than that of the previous work. Consequently, the specimens sintered at  $1350\text{ }^\circ\text{C}$  exhibited excellent properties, including an open porosity of  $53.2 \pm 0.5\%$  and a biaxial flexural strength of  $42.7 \pm 0.8\text{ MPa}$ . Furthermore, the mullite whiskers in the specimen were uniformly distributed and clustered, similar to a hedgehog, with a diameter of  $0.05\text{--}0.5\text{ }\mu\text{m}$ , length of  $8\text{--}10\text{ }\mu\text{m}$ , and aspect ratios (length to diameter ratio) of  $10\text{--}20$ , on average.

Figure 9 shows a peak of sound absorption in the low-frequency range between 630 and 2500 Hz. In the medium-frequency range, the sound absorption coefficient slightly decreased and then stayed at the same level with increasing frequency. The specimens with 12 wt.%  $\text{AlF}_3$  and 2 wt.%  $\text{CeO}_2$  had the highest sound absorption coefficients. The presence of lattice defects in  $\text{CeO}_2$  facilitated the release of oxygen atoms toward the activation center, resulting in the formation of a low-viscosity Ce-Al-Si-O liquid phase [38]. This liquid phase enhanced material diffusion and accelerated the creation of mullite whiskers. Consequently, porous ceramics exhibited a greater number of gas–solid interfaces, promoting enhanced reflection, scattering, and friction between sound waves and pore walls. This transformation led to the more efficient conversion of sound energy into heat energy [39]. Additionally, the even dispersion of whiskers across the surface of specimens contributed to increased surface roughness of the ceramic, further amplifying friction and reducing air viscosity [40].



**Figure 9.** Effect of the content of  $\text{AlF}_3$  and  $\text{CeO}_2$  on the sound absorption coefficient of the specimens.

Similar to Figure 9, all the curves of specimens in Figure 10 present the sound absorption coefficients of the A12C2 specimens sintered at  $1200\text{--}1350\text{ }^\circ\text{C}$  in the frequency range from 200 to 4000 Hz. Figure 10 shows a peak of sound absorption in the low-frequency range (200–2500 Hz), but then slightly decreased and remained stable at relatively higher frequencies. The sound absorption coefficient of the specimens sintered at  $1250\text{--}1350\text{ }^\circ\text{C}$  was higher than the specimen sintered at  $1200\text{ }^\circ\text{C}$ . The specimens sintered at  $1300\text{ }^\circ\text{C}$  had excellent sound absorption properties, i.e., a sound absorption coefficient of  $\geq 0.98$  between 1000 and 1600 Hz, and  $\geq 0.80$  between 2500 and 4000 Hz. A comparison of the data from this work with data reported in the literature is shown in Table 1.

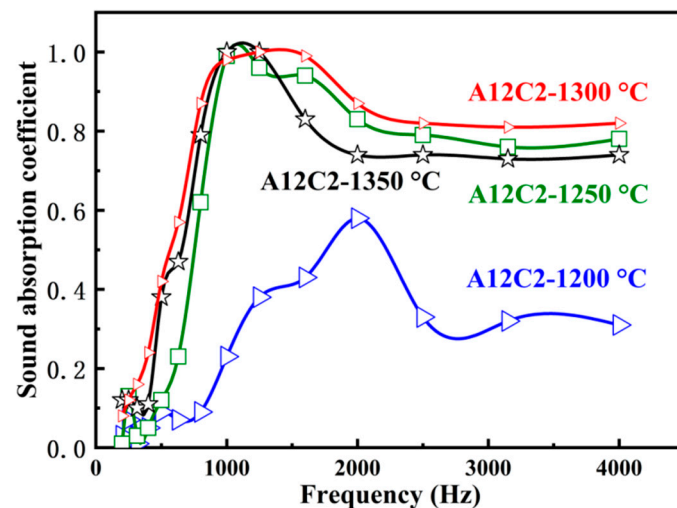


Figure 10. Effect of the sintering temperatures on sound absorption coefficient of the specimens.

Table 1. Performance comparison of porous sound-absorbing ceramics.

The Main Raw Material	Porosity (%)	Compressive Strength (MPa)	Frequency Range (Hz)	Sound Absorption Coefficient
Al <sub>2</sub> O <sub>3</sub> , ZrO <sub>2</sub> [41]	97.8–98.0	0.066–0.091	500–6500	0.60–0.77
SiC [42]	76–82	1.21–5.13	200–1600	<0.80
Na <sub>2</sub> B <sub>4</sub> O <sub>7</sub> ·10H <sub>2</sub> O [3]	-	1.12 ± 0.05	200–1400	<0.58
Al <sub>2</sub> O <sub>3</sub> /mullite [43]	77–82%	0.27–0.68	50–1400	0.30–0.99
This work	56.4 ± 0.6	-	800–4000	>0.80

Figure 11 shows the pore size distribution of sample A12C2 at different sintering temperatures. The average pore size distributions of the samples at 1250, 1300, and 1350 °C were all single-peaked, and they were 1.32, 1.32, and 2.54 μm, respectively, and the corresponding cumulative volume fractions were 15.7, 38.3, and 27.0%, respectively. Figure 11 shows that reducing the average pore size improved the acoustic absorption properties of the ceramic samples. When sound waves propagated to the surface of porous ceramics and entered the pores, they triggered the vibration of the air inside the pores. If the pore size is relatively small, the vibration is more likely to form a resonance effect. Resonance can more effectively convert acoustic energy into thermal energy, thus consuming the energy of the sound wave to achieve the effect of sound absorption. The pore structure of porous ceramics is regarded as a series of tiny Helmholtz resonators. As the pore size decreased, the area of the radial opening of the Helmholtz resonator also decreased, lowering the resonance frequency of the resonator. Therefore, as the pore size decreased, the absorption peak of porous ceramics moved toward lower frequencies, thus broadening the sound absorption frequency range. When sound waves propagated in smaller pore diameters, the energy of the sound waves was rapidly converted into heat energy due to the friction of the pore walls and the viscous resistance of the air [44].

In the frequency range of 1000–1600 Hz, the longer wavelength of the sound waves led to increased diffraction and scattering as the waves propagated through the porous ceramic. This process, combined with the friction between air molecules and the pore walls, led to the conversion of sound energy into internal energy or other forms of energy, improving sound absorption. Reducing the pore size of the porous ceramics enhanced the reflection of sound waves within the material, increasing the vibration of air molecules and the friction between these molecules and the pore walls [45,46]. However, from 2500 to 4000 Hz, the shorter wavelength of the sound waves implied that simple channels might not effectively capture and attenuate the high-frequency sound waves. If the pore size is relatively large compared to the high-frequency sound waves, the sound waves may be reflected inside the pores rather than being absorbed. This reflection would consequently diminish the

sound absorption effectiveness. The more pores inside the porous ceramics increased the reflection, scattering, and friction between the sound waves and the pore walls. Therefore, more acoustic energy was converted into thermal energy (Figure 12). The open porosity of the sintered specimens at 1300 °C was slightly lower than that of the sintered specimens at 1250 °C and 1200 °C (Figure 4). However, the acoustic absorption performance of the sintered specimens was better at 1300 °C than the sintered specimens at 1200 °C. This improved performance was attributed to the numerous micropores and microcracks in the sintered porous ceramic specimens at 1300 °C. The presence of micropores and microcracks increased friction and viscous air depletion, which improved the acoustic absorption performance [40].

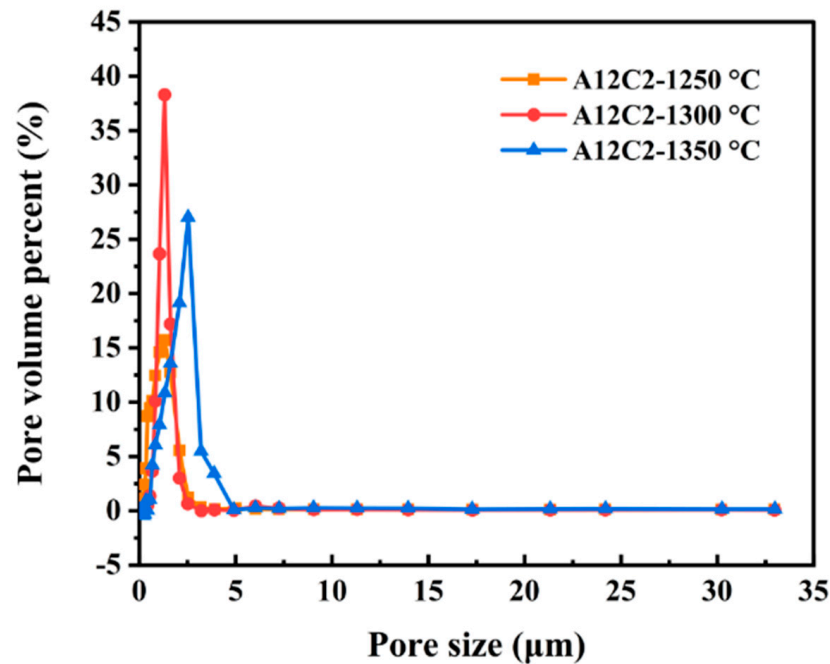


Figure 11. Effect of the sintering temperatures on the pore size distribution of the specimens.

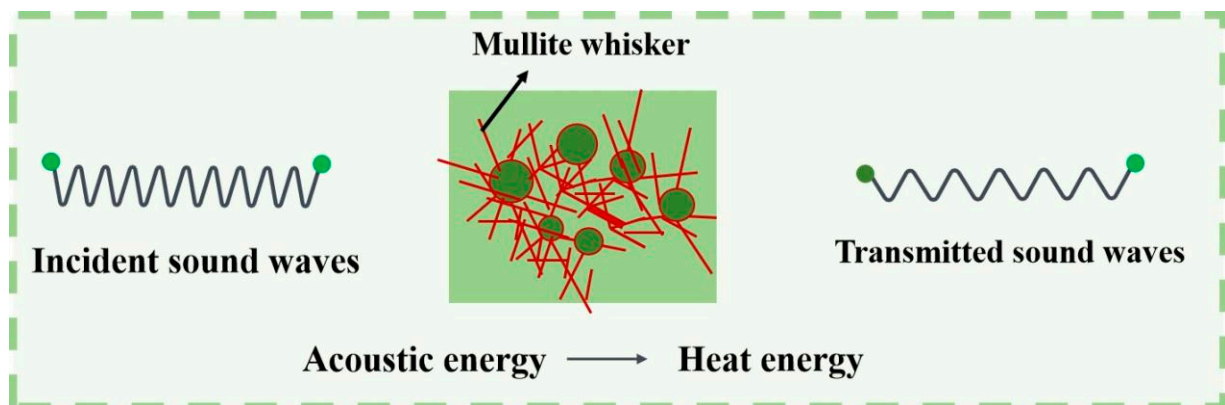


Figure 12. Demonstration diagram of sound absorption and noise reduction of porous ceramics.

### 3. Experimental

#### 3.1. Raw Materials for Porous Ceramics

The raw materials for this study were construction waste,  $\text{Al}_2\text{O}_3$ ,  $\text{AlF}_3 \cdot 3\text{H}_2\text{O}$ , and  $\text{CeO}_2$ . Construction waste was sourced from Guangzhou Shizheng Environment Co., Ltd. in Guangdong Province, China. This raw material underwent dry ball milling in a planetary ball mill (QM-ISP4-CL, Instrument Plant of Nanjing University. Dimensions:

570 × 380 × 450 mm, 100 mL corundum ball mill can). The sizes of zirconia ball milling beads were 1 mm<sup>3</sup>, 5 mm<sup>3</sup>, and 10 mm<sup>3</sup>, and the ratio of ball milling beads of each size was 3:5:2. The milling process was conducted at 300 rpm for 1 h, and sieved through a 0.6 mm sieve. The chemical composition of the construction waste was determined using the silicate chemical composition rapid analyzer (GKF-IV, Xiangtan Xiangyi Instrument Co., Ltd., Xiangtan, China). As shown in Table 2, the chemical compositions are 71.65 wt.% SiO<sub>2</sub> and 7.67 wt.% Al<sub>2</sub>O<sub>3</sub>.

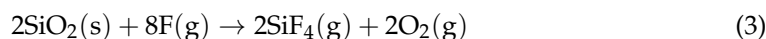
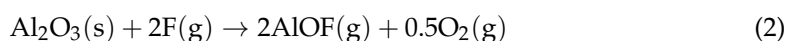
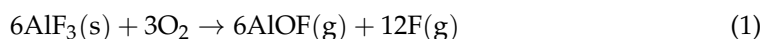
**Table 2.** Main chemical composition (wt.%) of the construction waste.

Materials	Chemical Composition (wt.%)								
	LI	SiO <sub>2</sub>	Al <sub>2</sub> O <sub>3</sub>	Fe <sub>2</sub> O <sub>3</sub>	TiO <sub>2</sub>	CaO	MgO	K <sub>2</sub> O	Na <sub>2</sub> O
Construction waste	6.36	71.65	7.67	1.71	0.21	9.20	0.62	1.97	0.79

Note: LI stands for loss of ignition.

### 3.2. Fabrication of Porous Ceramics

Al<sub>2</sub>O<sub>3</sub> powder (AR, Chinasun Specialty Products Co., Ltd., Changshu, China) was used as the alumina source (presented as 3Al<sub>2</sub>O<sub>3</sub>·2SiO<sub>2</sub>) to produce the mullite reinforcement due to the inadequate amounts of aluminum in the construction waste. AlF<sub>3</sub>·3H<sub>2</sub>O (98.0–102.0%, Sinopharm Chemical Reagent Co., Ltd., Shanghai, China) and CeO<sub>2</sub> (99.99%, Sinopharm Chemical Reagent Co., Ltd., Shanghai, China) were used as the crystallization catalyst and sintering aids, respectively. AlF<sub>3</sub> played the following dual roles: promoting mullite whisker formation (by transforming to Al<sub>2</sub>O<sub>3</sub> and the subsequent reaction with SiO<sub>2</sub>) and serving as a partial aluminum source for forming stoichiometric 3:2 mullite. In the Al<sub>2</sub>O<sub>3</sub>-SiO<sub>2</sub>-AlF<sub>3</sub> system, the chemical process to generate mullite proceeded as follows [47]:



A series of porous ceramics were synthesized using the stoichiometric mullite composition with varying AlF<sub>3</sub> and CeO<sub>2</sub> content. In this study, these ceramics were designated as AxCy, where A represents AlF<sub>3</sub>, C represents CeO<sub>2</sub>, and x and y indicate the respective mass percentages of each compound in the raw materials of the samples. Detailed compositions are provided in Table 3.

**Table 3.** Mixing ratio of raw materials.

Sample ID	Construction Waste (wt.%)	Content of Al <sub>2</sub> O <sub>3</sub> (wt.%)	Content of CeO <sub>2</sub> (wt.%)	Content of AlF <sub>3</sub> (wt.%)
A0C0	29.08	70.92	0	0
A12C0	25.59	62.41	0	12
A12C1	25.30	61.70	1	12
A12C2	25.01	60.99	2	12
A12C3	24.72	60.28	3	12
A12C4	24.43	59.57	4	12

### 3.3. Characterization and Test

The phases of the construction waste and the sintered specimens were analyzed via powder X-ray diffraction (XRD; X'Pert Pro, PANalytical Co., Almelo, Holland) with Cu Kα radiation (λ = 0.15418 nm), using graphite monochromatization. Operating parameters included a tube voltage of 40 kV, a tube current of 40 mA, a 2θ angle step size of 0.0330°, a

scan step time of 10.160 s, and a  $2\theta$  angle scan range from  $10^\circ$  to  $90^\circ$ . The open porosity and bulk density of the sintered specimens (which corresponded to rectangular green pieces measuring  $5\text{ mm} \times 20\text{ mm} \times 48\text{ mm}$ ) were determined using Archimedes' method as per ASTM C 20-92, using distilled water as the immersion medium. Each specimen underwent ten parallel measurements, with each measurement repeated five times, and the average result was recorded as the measured value of the specimen.

The biaxial flexural strength of the sintered specimens was evaluated using an electronic digital control system (INSTRON-5567, Co. Instron Engineering Corporation, Boston, USA) through the three-point bending test [35,36], conducted at room temperature. Standardized specimens ( $3\text{ mm} \times 4\text{ mm} \times 35\text{ mm}$ ) were polished and subjected to a 30 mm span at a loading rate of 0.5 mm/min. Each specimen was tested in eight parallels, and the average measurement results were recorded. The microstructures of the sintered specimens were examined using scanning electron microscopy (Nova Nano SEM 430, FEI, Hillsboro, OR, USA). The sound absorption coefficient of the sintered specimens ( $100\text{ mm} \times 50\text{ mm} \times 10\text{ mm}$ ) was determined. The 100 mm diameter specimen was used to assess sound absorption coefficients for lower frequencies (200–2000 Hz), while the 50 mm diameter specimen was used for higher frequencies (2500–4000 Hz). The test was conducted using the JTZB-type system (Beijing Century Jiantong Technology Development Limited Company, Beijing, China) and the standing wave tube method, following ASTM E 1050-98. Additionally, the transfer function methodology was used as specified in the EN ISO 10534-2 standard. The sound absorption coefficient ( $\alpha$ ) was calculated using the following Equations (5) and (6):

$$\alpha = \frac{4n}{(1+n)^2} \quad (5)$$

$$n = \frac{|p_{max}|}{|p_{min}|} \quad (6)$$

where  $n$  is the standing wave ratio, and  $p_{max}$  and  $p_{min}$  are the maximum and minimum sound pressures in the impedance tube, respectively.

The ceramic sample line shrinkage  $S_0$  (%) is calculated as follows in Equation (7):

$$S_0 = \frac{L_0 - L}{L_0} \quad (7)$$

where  $L_0$  is the sample length before sintering, and  $L$  is the sample length after sintering.

#### 4. Conclusions

In situ mullite whisker-reinforced porous sound-absorbing ceramics with high strength were successfully prepared with construction waste and  $\text{Al}_2\text{O}_3$  powder as the raw materials, and  $\text{AlF}_3$  and  $\text{CeO}_2$  as the additives and mineralizing agents, respectively. A small amount of  $\text{CeO}_2$  effectively enhanced the growth of elongated mullite crystals in the porous ceramics, decreased the growth temperature of the mullite whiskers, and increased the biaxial flexural strength of the specimen, whereas excessive  $\text{CeO}_2$  inhibited the mullitization. By co-adding 2 wt.%  $\text{CeO}_2$  and 12 wt.%  $\text{AlF}_3$  in the system, mullite whiskers were successfully obtained at a sintering temperature of  $1300^\circ\text{C}$  for 1 h. The obtained mullite whiskers exhibited excellent properties, including an open porosity of  $56.4 \pm 0.6\%$ , an average pore size of  $1.32\text{--}2.54\ \mu\text{m}$ , a biaxial flexural strength of  $23.7 \pm 0.9\ \text{MPa}$ , and a sound absorption coefficient of  $> 0.8$  at 800–4000 Hz. This work offers a cost-effective method for the future preparation of high-performance, porous, sound-absorbing ceramics from construction waste.

**Author Contributions:** Conceptualization, A.S. and X.X.; methodology, K.H.; software, X.C. and K.H.; validation, A.S., X.X. and Y.Z.; formal analysis, X.C.; investigation, K.H. and P.G.; resources, A.S. and X.X.; data curation, K.H.; writing—original draft preparation, K.H.; writing—review and editing, X.C., K.H. and X.X.; visualization, P.G. and C.H.; supervision, A.S., X.X. and Y.Z.; project

administration, A.S., X.X., Y.Z. and K.H.; funding acquisition, A.S., X.X.. All authors have read and agreed to the published version of the manuscript.

**Funding:** This work was supported by [the National Natural Science Foundation of China] grant number [52272062]; [the Guangdong Basic and Applied Basic Research Foundation for Guangdong-Dongguan Joint Funding Project] [2023A1515140095]; the Dongguan Social Science and Technology Development (Major) Project grant number [20211800905302]; [the Guangdong-Macao Joint Funding Topic of Science and Technology Innovation] grant number [2022A0505020030]; [the International Science and Technology Innovation Center Construction Fund Project of the Guangdong-Hong Kong-Macao Greater Bay Area, China] grant number [2021A0505110016]; [the Guangdong Provincial Key Laboratory of Intelligent Disaster Prevention and Emergency Technologies for Urban Lifeline Engineering] grant number [2022B1212010016]; [the Natural Science Foundation of China] grant number [52178192]; [the Talent Training Project of Guangdong Joint Graduate Training Demonstration Base] grant number [Guangdong Education Research Letter [2021] No. 2, [2023] No. 3]; [the Songshan Lake Special Agent Project] grant number [20234418-01KCJ-G]; [the Quality Engineering Project of Dongguan University of Technology] grant number [202302031]; [Guangdong Basic and Applied Basic Research Foundation] grant number [2020A1515110081]; and [the Guangdong Basic and Applied Basic Research Foundation] grant number [2021A1515110723].

**Data Availability Statement:** The original contributions presented in the study are included in the article, further inquiries can be directed to the corresponding author/s.

**Acknowledgments:** The SEM images data were obtained using equipment maintained by the Dongguan University of Technology Analytical and Testing Center.

**Conflicts of Interest:** The authors declare no conflicts of interest.

## References

1. Guenka, T.S.N.; Machado, M.R.; Silva, A.M.A.; Nunes, M.A.A. Freeze-cast porous Al<sub>2</sub>O<sub>3</sub>/MgO ceramics as potential acoustic sound absorption. *Appl. Acoust.* **2024**, *220*, 109964. [[CrossRef](#)]
2. Li, X.; Peng, Y.; He, Y.; Zhang, C.; Zhang, D.; Liu, Y. Research Progress on Sound Absorption of Electrospun Fibrous Composite Materials. *Nanomater.* **2022**, *12*, 1123. [[CrossRef](#)] [[PubMed](#)]
3. He, C.; Shui, A.; Ma, J.; Qian, J.; Cai, M.; Tian, W.; Du, B. In situ growth magnesium borate whiskers and synthesis of porous ceramics for sound-absorbing. *Ceram. Int.* **2020**, *46*, 29339–29343. [[CrossRef](#)]
4. Oancea, I.; Bujoreanu, C.; Budescu, M.; Benchea, M.; Grădinaru, C.M. Considerations on sound absorption coefficient of sustainable concrete with different waste replacements. *J. Clean. Prod.* **2018**, *203*, 301–312. [[CrossRef](#)]
5. Arenas, C.; Luna-Galiano, Y.; Leiva, C.; Vilches, L.F.; Arroyo, F.H.; Villegas, R.; Fernández-Pereira, C.J.C.; Materials, B. Development of a fly ash-based geopolymeric concrete with construction and demolition wastes as aggregates in acoustic barriers. *Constr. Build. Mater.* **2017**, *134*, 433–442. [[CrossRef](#)]
6. Hua, K.; Shui, A.; Xu, L.; Zhao, K.; Zhou, Q.; Xi, X. Fabrication and characterization of anorthite–mullite–corundum porous ceramics from construction waste. *Ceramics International* **2016**, *42*, 6080–6087. [[CrossRef](#)]
7. Huang, B.; Miao, Q.; Zuo, X.; Yi, J.; Zhou, Y.; Luo, X. Sound absorption performance and mechanism of aluminum foam with double-layer structures of conventional and porous cell walls. *Appl. Acoust.* **2024**, *222*, 110054. [[CrossRef](#)]
8. Wu, L.; Li, C.; Chen, Y.; Wang, C.-a. Seed assisted in-situ synthesis of porous anorthite/mullite whisker ceramics by foam-freeze casting. *Ceram. Int.* **2021**, *47*, 11193–11201. [[CrossRef](#)]
9. Chen, J.H.; Liu, P.S.; Sun, J.X. Sound absorption performance of a lightweight ceramic foam. *Ceram. Int.* **2020**, *46*, 22699–22708. [[CrossRef](#)]
10. Du, Z.; Yao, D.; Xia, Y.; Zuo, K.; Yin, J.; Liang, H.; Zeng, Y.-P. Highly porous silica foams prepared via direct foaming with mixed surfactants and their sound absorption characteristics. *Ceram. Int.* **2020**, *46*, 12942–12947. [[CrossRef](#)]
11. Gao, X.; Zhang, D.; Feng, X.; Zhang, J.; Yuqing, P.; Zhicheng, P.; Zongming, D. Effect of particle size of associated rare earth kaolin powder on the sintering and properties of synthetic mullite. *J. Am. Ceram. Soc.* **2024**, *107*, 2658–2667. [[CrossRef](#)]
12. Cheng, X.; Ke, S.; Wang, Q.; Wang, H.; Shui, A.; Liu, P. Fabrication and characterization of anorthite-based ceramic using mineral raw materials. *Ceram. Int.* **2012**, *38*, 3227–3235. [[CrossRef](#)]
13. Xu, L.; Xi, X.; Shui, A.; Zhu, W. Preparation of mullite whisker skeleton porous ceramic. *Ceram. Int.* **2015**, *41*, 11576–11579. [[CrossRef](#)]
14. Hua, K.; Xi, X.; Xu, L.; Zhao, K.; Wu, J.; Shui, A. Effects of AlF<sub>3</sub> and MoO<sub>3</sub> on properties of Mullite whisker reinforced porous ceramics fabricated from construction waste. *Ceram. Int.* **2016**, *42*, 17179–17184. [[CrossRef](#)]
15. Zhu, L.; Dong, Y.; Li, L.; Liu, J.; You, S.-J. Coal fly ash industrial waste recycling for fabrication of mullite-whisker-structured porous ceramic membrane supports. *RSC Adv.* **2015**, *5*, 11163–11174. [[CrossRef](#)]
16. Li, C.; Zhou, Y.; Tian, Y.; Zhao, Y.; Wang, K.; Li, G.; Chai, Y. Preparation and characterization of mullite whisker reinforced ceramics made from coal fly ash. *Ceram. Int.* **2019**, *45*, 5613–5616. [[CrossRef](#)]

17. Wang, J.; Wu, H.; Tam, V.W.Y.; Zuo, J. Considering life-cycle environmental impacts and society's willingness for optimizing construction and demolition waste management fee: An empirical study of China. *J. Clean. Prod.* **2019**, *206*, 1004–1014. [[CrossRef](#)]
18. Li, Z.; Sun, J.; Zhang, X.; Zhang, J.; Han, G. In-situ mullite whisker reinforced SiC porous ceramics with whiskers and bonding layers synchronously growing: Using CaF<sub>2</sub> as a temperature-controlled whisker formation switch. *J. Eur. Ceram. Soc.* **2024**, *44*, 3470–3478. [[CrossRef](#)]
19. Zhang, H.; Tang, J.; Zhang, Y.; Huang, C.; Wu, H.; Yuan, M.; Liu, X.; Huang, Z. Cross-scale construction of SiC–Si<sub>3</sub>N<sub>4</sub> porous ceramics with superior electromagnetic wave absorption performance. *Ceram. Int.* **2024**, *50*, 2177–2184. [[CrossRef](#)]
20. Wang, W.; Liu, H.; Gu, W. A novel fabrication approach for improving the mechanical and sound absorbing properties of porous sound-absorbing ceramics. *J. Alloys Compd.* **2017**, *695*, 2477–2482. [[CrossRef](#)]
21. Yang, M.; Li, J.; Man, Y.; Peng, Z.; Zhang, X.; Luo, X. A three-dimensional mullite-whisker network ceramic with ultra-light weight and high-strength prepared by the foam-gelcasting method. *J. Asian Ceram. Soc.* **2020**, *8*, 387–395. [[CrossRef](#)]
22. Roy, J.; Bandyopadhyay, N.; Das, S.; Maitra, S. Role of V<sub>2</sub>O<sub>5</sub> on the formation of chemical mullite from aluminosilicate precursor. *Ceram. Int.* **2010**, *36*, 1603–1608. [[CrossRef](#)]
23. Zhu, Z.; Wei, Z.; Shen, J.; Zhu, L.; Xu, L.; Zhang, Y.; Wang, S.; Liu, T. Fabrication and catalytic growth mechanism of mullite ceramic whiskers using molybdenum oxide as catalyst. *Ceram. Int.* **2017**, *43*, 2871–2875. [[CrossRef](#)]
24. Mahnicka-Goremikina, L.; Svinka, R.; Svinka, V. Influence of ZrO<sub>2</sub> and WO<sub>3</sub> doping additives on the thermal properties of porous mullite ceramics. *Ceram. Int.* **2018**, *44*, 16873–16879. [[CrossRef](#)]
25. Wang, X.; Li, J.; Tong, L.X.; Feng, W.J.C.I. Phase evolution and dynamics of cerium-doped mullite whiskers synthesized by sol-gel process. *Ceram. Int.* **2013**, *39*, 9677–9681. [[CrossRef](#)]
26. Ji, S.J.; Guo, X.Y.; Dong, J.X.; Su, P. Effects of CeO<sub>2</sub>-Rich Mixed Rare Earth on the Mechanical Properties of Al<sub>2</sub>O<sub>3</sub>-Mullite Based Foam Ceramics. *Adv. Mater. Res.* **2011**, *150*, 815–820. [[CrossRef](#)]
27. Wu, J.-M.; Lin, C.-M. Effect of CeO<sub>2</sub> on reaction-sintered mullite-ZrO<sub>2</sub> ceramics. *J. Mater. Sci.* **1991**, *26*, 4631–4636. [[CrossRef](#)]
28. Huo, X.; Xia, B.; Hu, T.; Zhang, M.; Guo, M. Effect of MoO<sub>3</sub> addition on fly ash based porous and high-strength mullite ceramics: In situ whisker growth and self-enhancement mechanism. *Ceram. Int.* **2023**, *49*, 21069–21077. [[CrossRef](#)]
29. Liu, R.; Xiang, D. Recycling photovoltaic silicon waste for fabricating porous mullite ceramics by low-temperature reaction sintering. *J. Eur. Ceram. Soc.* **2021**, *41*, 5957–5966. [[CrossRef](#)]
30. Lin, S.-M.; Yu, Y.-L.; Zhong, M.-F.; Yang, H.; Liu, Y.; Li, H.; Zhang, C.-Y.; Zhang, Z.-J. Preparation of Anorthite/Mullite in Situ and Phase Transformation in Porcelain. *Mater.* **2023**, *16*, 1616. [[CrossRef](#)]
31. Li, K.; Ge, S.; Yuan, G.; Zhang, H.; Zhang, J.; He, J.; Jia, Q.; Zhang, S. Effects of V<sub>2</sub>O<sub>5</sub> addition on the synthesis of columnar self-reinforced mullite porous ceramics. *Ceram. Int.* **2021**, *47*, 11240–11248. [[CrossRef](#)]
32. Behera, P.S.; Bhattacharyya, S. Effect of different alumina sources on phase formation and densification of single-phase mullite ceramic – Reference clay alumina system. *Mater. Today Commun.* **2021**, *26*, 101818. [[CrossRef](#)]
33. Rana, A.P.S.; Aiko, O.; Pask, J.A. Sintering of  $\alpha$ -Al<sub>2</sub>O<sub>3</sub>/quartz, and  $\alpha$ -Al<sub>2</sub>O<sub>3</sub>/cristobalite related to mullite formation. *Ceram. Int.* **1982**, *8*, 151–153. [[CrossRef](#)]
34. Wu, C.; Shu, P.; Zhan, L.; Zhang, X.; Wang, J.; Liu, W.; Yao, S.; Ma, Y. Development and strategy of alumina-mullite diphasic fibers with high thermal stability. *J. Eur. Ceram. Soc.* **2024**, *44*, 4045–4054. [[CrossRef](#)]
35. Yan, L.L.; Han, B.; Yu, B.; Chen, C.Q.; Zhang, Q.C.; Lu, T.J. Three-point bending of sandwich beams with aluminum foam-filled corrugated cores. *Mater. Des.* **2014**, *60*, 510–519. [[CrossRef](#)]
36. Gupta, N.; Woldesenbet, E.; Kishore; Sankaran, S. Response of Syntactic Foam Core Sandwich Structured Composites to Three-Point Bending. *J. Sandw. Struct. Mater.* **2002**, *4*, 249–272. [[CrossRef](#)]
37. Sacks, M.D.; Lin, Y.-J.; Scheiffele, G.W.; Wang, K.; Bozkurt, N. Effect of Seeding on Phase Development, Densification Behavior, and Microstructure Evolution in Mullite Fabricated from Microcomposite Particles. *J. Am. Ceram. Soc.* **1995**, *78*, 2897–2906. [[CrossRef](#)]
38. Regiani, I.; Magalhães, W.L.E.; De Souza, D.P.F.; Paiva-Santos, C.O.; De Souza, M.F. Nucleation and Growth of Mullite Whiskers from Lanthanum-Doped Aluminosilicate Melts. *J. Am. Ceram. Soc.* **2002**, *85*, 232–238. [[CrossRef](#)]
39. Mechnich, P.; Schneider, H.; Schmücker, M.; Saruhan, B. Accelerated Reaction Bonding of Mullite. *J. Am. Ceram. Soc.* **1998**, *81*, 1931–1937. [[CrossRef](#)]
40. Pakdel, E.; Naebe, M.; Kashi, S.; Cai, Z.; Xie, W.; Yuen, A.C.Y.; Montazer, M.; Sun, L.; Wang, X. Functional cotton fabric using hollow glass microspheres: Focus on thermal insulation, flame retardancy, UV-protection and acoustic performance. *Prog. Org. Coat.* **2020**, *141*, 105553. [[CrossRef](#)]
41. Dong, X.; An, Q.; Zhang, S.; Yu, H.; Wang, M. Porous ceramics based on high-thermal-stability Al<sub>2</sub>O<sub>3</sub>–ZrO<sub>2</sub> nanofibers for thermal insulation and sound absorption applications. *Ceram. Int.* **2023**, *49*, 31035–31045. [[CrossRef](#)]
42. Lou, J.; He, C.; Shui, A.; Yu, H. Enhanced sound absorption performance of porous ceramics with closed-pore structure. *Ceramics International* **2023**, *49*, 38103–38114. [[CrossRef](#)]
43. Carlesso, M.; Giacomelli, R.; Günther, S.; Koch, D.; Kroll, S.; Odenbach, S.; Rezwan, K. Near-Net-Shaped Porous Ceramics for Potential Sound Absorption Applications at High Temperatures. *J. Am. Ceram. Soc.* **2013**, *96*, 710–718. [[CrossRef](#)]
44. Trinh, V.H.; Langlois, V.; Guilleminot, J.; Perrot, C.; Khidas, Y.; Pitois, O. Tuning membrane content of sound absorbing cellular foams: Fabrication, experimental evidence and multiscale numerical simulations. *Mater. Des.* **2019**, *162*, 345–361. [[CrossRef](#)]
45. Xu, Z.; He, W.; Xin, F.; Lu, T.J. Sound propagation in porous materials containing rough tubes. *Phys. Fluids* **2020**, *32*, 093604. [[CrossRef](#)]

46. Yang, F.; Zhao, S.; Sun, W.; Li, K.; Chen, J.; Fei, Z.; Yang, Z. Fibrous porous mullite ceramics modified by mullite whiskers for thermal insulation and sound absorption. *J. Eur. Ceram. Soc.* **2023**, *43*, 521–529. [[CrossRef](#)]
47. Yi, P.; Zhao, P.; Zhang, D.; Zhang, H.; Zhao, H. Preparation and characterization of mullite microspheres based porous ceramics with enhancement of in-situ mullite whiskers. *Ceram. Int.* **2019**, *45*, 14517–14523. [[CrossRef](#)]

**Disclaimer/Publisher’s Note:** The statements, opinions and data contained in all publications are solely those of the individual author(s) and contributor(s) and not of MDPI and/or the editor(s). MDPI and/or the editor(s) disclaim responsibility for any injury to people or property resulting from any ideas, methods, instructions or products referred to in the content.